Received: 18 July 2019 | Accepted: 21 September 2019

DOI: 10.1111/gcb.14888

PRIMARY RESEARCH ARTICLE

Global Change Biology WILEY

Climate change decreases the cooling effect from postfire albedo in boreal North America

Stefano Potter[1] | Kylen Solvik[1,2] | Angela Erb[3] | Scott J. Goetz[4] | Jill F. Johnstone[5] | Michelle C. Mack[6] | James T. Randerson[7] | Miguel O. Román[8] | Crystal L. Schaaf[3] | Merritt R. Turetsky[9] | Sander Veraverbeke[10] | Xanthe J. Walker[6] | Zhuosen Wang[8,11] | Richard Massey[4] | Brendan M. Rogers[1]

[1]Woods Hole Research Center, Falmouth, MA, USA

[2]Geography Department, University of Colorado, Boulder, CO, USA

[3]School for the Environment, University of Massachusetts Boston, Boston, MA, USA

[4]School of Informatics, Computing, and Cyber Systems, Northern Arizona University, Flagstaff, AZ, USA

[5]UAF: Institute of Arctic Biology, University of Alaska Fairbanks, Fairbanks, AL, USA

[6]Center for Ecosystem Science and Society, Northern Arizona University, Flagstaff, AZ, USA

[7]Department of Earth System Science, University of California, Irvine, CA, USA

[8]Earth from Space Institute, Universities Space Research Association, Columbia, MD, USA

[9]Department of Integrative Biology, University of Guelph, Guelph, ON, Canada

[10]Faculty of Science, Vrije Universiteit Amsterdam, Amsterdam, The Netherlands

[11]Earth System Science Interdisciplinary Center, University of Maryland, College Park, MD, USA

Correspondence
Stefano Potter, Woods Hole Research Center, Falmouth, MA, USA.
Email: spotter@whrc.org

Funding information
National Aeronautics and Space Administration, Grant/Award Number: NNX14AI73G and NNX15AU56A

Abstract

Fire is a primary disturbance in boreal forests and generates both positive and negative climate forcings. The influence of fire on surface albedo is a predominantly negative forcing in boreal forests, and one of the strongest overall, due to increased snow exposure in the winter and spring months. Albedo forcings are spatially and temporally heterogeneous and depend on a variety of factors related to soils, topography, climate, land cover/vegetation type, successional dynamics, time since fire, season, and fire severity. However, how these variables interact to influence albedo is not well understood, and quantifying these relationships and predicting postfire albedo becomes increasingly important as the climate changes and management frameworks evolve to consider climate impacts. Here we developed a MODIS-derived 'blue sky' albedo product and a novel machine learning modeling framework to predict fire-driven changes in albedo under historical and future climate scenarios across boreal North America. Converted to radiative forcing (RF), we estimated that fires generate an annual mean cooling of -1.77 ± 1.35 W/m^2 from albedo under historical climate conditions (1971–2000) integrated over 70 years postfire. Increasing postfire albedo along a south–north climatic gradient was offset by a nearly opposite gradient in solar insolation, such that large-scale spatial patterns in RF were minimal. Our models suggest that climate change will lead to decreases in mean annual postfire albedo, and hence a decreasing strength of the negative RF, a trend dominated by decreased snow cover in spring months. Considering the range of future climate scenarios and model uncertainties, we estimate that for fires burning in the current era (2016) the cooling effect from long-term postfire albedo will be reduced by 15%–28% due to climate change.

KEYWORDS

ABoVE, biophysics, climate feedback, energy budget, land/fire management, MODIS, succession

1 | INTRODUCTION

Land–atmosphere energy exchange across the boreal forest, the Earths largest terrestrial biome, has the potential to significantly influence global climate through disturbance-driven changes in forest cover (Bonan, Pollard, & Thompson, 1992). Fire frequency and burned area have been increasing in Alaskan and Canadian boreal forests (Gillett, Weaver, Zwiers, & Flannigan, 2004; Kasischke et al., 2010; Veraverbeke et al., 2017), and these trends are expected to continue throughout the 21st century due to a warmer and drier climate (Balshi et al., 2009a; Boulanger, Parisien, & Wang, 2018; Young, Higuera, Duffy, & Hu, 2017). Fire is the dominant disturbance mechanism in boreal forests (Stocks et al., 2002), and shifts in future fire regimes are likely to alter forest dynamics including vegetation composition (Johnson, 1992; Johnstone et al., 2010; Payette, 1992; Viereck, 1973) and carbon cycling (Balshi et al., 2009b; Genet et al., 2013). Boreal fires initiate both positive (+) and negative (−) climate feedbacks by emitting greenhouse gases (+; Amiro et al., 2001; Bond-Lamberty, Peckham, Ahl, & Gower, 2007) and carbonaceous aerosols during combustion (+ and −; Flanner, Zender, Randerson, & Rasch, 2007; Mouteva et al., 2015; Ward et al., 2012), reaccumulating carbon during postfire regrowth (−; Alexander & Mack, 2016; Amiro et al., 2010; Goulden et al., 2011), degrading permafrost which releases CO_2 and CH_4 (+; Brown et al., 2016; Jafarov, Romanovsky, Genet, McGuire, & Marchenko, 2013; Jorgenson et al., 2010), and altering the surface energy balance, primarily through albedo (−; Amiro et al., 2006; French, Whitley, & Jenkins, 2016; Randerson et al., 2006; Rogers, Randerson, & Bonan, 2013).

Postfire surface albedo changes are typically large in North American boreal forests (O'Halloran et al., 2012; Randerson et al., 2006). North American boreal forest fires are generally stand-replacing crown fires (de Groot et al., 2013; Johnson, Miyanishi, & Weir, 1998; Rogers, Soja, Goulden, & Randerson, 2015) that increase postfire albedo during the fall, winter and spring due to increased snow exposure (Amiro et al., 2006; Jin, Randerson, Goulden, & Goetz, 2012; Liu & Randerson, 2008; Wang, Erb, et al., 2016). Albedo peaks roughly 10–15 years after fire as dead snags fall and expose underlying snow, and regrowing vegetation is still relatively short (Jin et al., 2012; O'Halloran, Acker, Joerger, Kertis, & Law, 2014). In the summer, postfire albedo initially decreases due to deposition of black carbon on the soil surface and remaining boles. Nonetheless, this effect is short-lived and after roughly the first 5 years after fire, albedo increases as vegetation re-establishes, and can exceed prefire levels if shrubs and deciduous trees colonize and replace darker conifers (Chambers & Chapin, 2002; Randerson et al., 2006; Yoshikawa, Bolton, Romanovsky, Fukuda, & Hinzman, 2002).

Despite the importance of changing boreal wildfires on global climate, studies on the net climate effects have varied. A foundational study estimated the radiative forcings (RF) from a series of fires in interior Alaska, showing a net cooling effect due to the dominant influence of winter and spring albedo relative to greenhouse gas and aerosol emissions (Randerson et al., 2006). In a field-based study in central Canada, net climate effects were estimated as closer to neutral (O'Halloran et al., 2012), while Oris, Asselin, Ali, Finsinger, and Bergeron (2013) suggested that net forcings from fires in boreal North America may be positive. One of the primary uncertainties comes from the high spatial variability in fire effects, including carbon emissions (Rogers et al., 2014; Veraverbeke, Rogers, & Randerson, 2015; Walker et al., 2018) and albedo (Jin et al., 2012; Rogers et al., 2015; Wang, Erb, et al., 2016). Given this, multidecadal forcings are likely highly spatially variable, depending on complex interactions between climate, soils, topography, permafrost, vegetation, fire severity, and successional dynamics. Determining how these parameters influence postfire albedo at the landscape scale is critical for estimating the regional and global climate feedbacks from increased burning in Alaska and Canada.

Local environmental and ecological variables influence postfire albedo and the resulting RF in a variety of ways. Initial recruitment strongly controls postfire vegetation composition (Johnson, Miyanishi, & Kleb, 1994; Johnstone et al., 2010; Shenoy, Johnstone, Kasischke, & Kielland, 2011), and most importantly for albedo, initial recruitment may determine whether the regrowing vegetation is dominated by dark conifers or more reflective deciduous broadleaf trees, which is especially influential in winter and spring before leaf onset (Beck et al., 2011; Rogers et al., 2013). Recruitment, in turn, is strongly dependent on prefire vegetation, climate, soils, topographic position, disturbance history, and postfire organic layer depth and the exposure of mineral soil (Brown & Johnstone, 2012; de Groot et al., 2004; Whitman, Parisien, Thompson, & Flannigan, 2018). Large-scale climate patterns also impact postfire albedo through controls on successional dynamics (Trugman et al., 2016), canopy structure (Abis & Brovkin, 2017; Hovi, Liang, Korhonen, Kobayashi, & Rautiainen, 2016), snow extent (Atlaskina, Berninger, & de Leeuw, 2015; Chen, Liang, Cao, He, & Wang, 2015; Li, Ma, Wu, & Yang, 2018), and particularly the timing of spring melt. Moreover, cloud patterns and latitudinal gradients in solar insolation influence the RF from a given change in surface albedo (Jin et al., 2012; Shell et al., 2008). Thus, determining the net effect of fire on albedo and RF requires consideration of both temporal variation (e.g., among seasons and with year-since-fire) and spatial variation in climate, topo-edaphic conditions, and insolation.

Prior studies assessing the influence of postfire albedo on climate have focused primarily on individual fire events or groups of fires in specific locations, thereby neglecting the continental-scale spatial variability in albedo, its drivers, and the resulting RF, and especially how these dynamics may change in the future. Moreover, a majority of prior efforts have used remote sensing-based albedo products that (a) represent multiweek composites, which do not accurately capture periods of rapid transition such as snow melt (Wang et al., 2012) and (b) neglect the influence of multiple photon scattering, which is particularly influential under conditions of high albedo and large solar zenith angles (i.e., anisotropic diffuse illumination during winter and spring in high latitudes; e.g., Román et al., 2010) and leads to an underestimation of albedo (Román et al., 2010; Wang et al., 2012, 2014). Gaining a better and more accurate understanding of postfire albedo patterns is critical for determining the net climate feedback from fires in boreal North America, currently and in the future under continued climate changes and intensified fire regimes.

In this study we used a data-driven statistical modeling approach to (a) identify influential variables that drive postfire albedo in different seasons across boreal North America, (b) model long-term trajectories of postfire albedo as a function of these drivers, (c) calculate the RF from fire-induced albedo changes, (d) assess the large-scale spatial variation in albedo trajectories and RF, and (e) estimate how albedo-driven RF may change under future climate scenarios.

2 | METHODS

We used random forest regression (Breiman, 2001) to model monthly postfire albedo across Canada and Alaska at 500 m resolution based on a suite of predictor variables including year-since-fire, climate, and properties related to soils, topography, and permafrost. The resulting models were used to predict albedo and the associated RF under historical and future climate scenarios.

2.1 | Study area and fire history

Our study domain included natural boreal vegetation across Alaska and Canada. To distinguish the desired land cover, we derived a vegetation mask using the 2005 Land Cover of North America product (250 m; CCRS, 2013; Pouliot & Latifovic, 2013; Pouliot, Latifovic, Zabcic, Guindon, & Olthof, 2014), Moderate Resolution Imaging Spectroradiometer (MODIS) land cover type with IGBP classification (Collection 5; year 2005; 500 m; Friedl et al., 2010), the Circumpolar Arctic Vegetation Map (CAVM; CAVM Team, 2003), and long-term climate (1950–2000; ~1 km; Hijmans, Cameron, Parra, Jones, & Jarvis, 2005), all regridded to 500 m resolution on the MODIS sinusoidal projection. Boreal vegetation was distinguished from temperate using a mean annual temperature threshold of 3°C, as recommended in Wolfe (1979) and implemented in Rogers et al. (2015). CAVM was used to define the boundary between boreal and tundra vegetation. To be conservative about our inclusion of vegetated pixels, we excluded pixels designated as urban, crop, ice/barren, or water in either the Land Cover of North America or the MODIS IGBP land cover product.

Because we were interested in long-term albedo dynamics, it was essential to use a fire record that spanned a longer time series than products derived purely from the remote sensing record (e.g., Landsat or MODIS). We therefore used the Alaska Large Fire Database (ALFD; Kasischke, Williams, & Barry, 2002) and Canadian National Fire Database (CNFD; Amiro et al., 2001; Stocks et al., 2002). Although fires date back to 1940 in the ALFD and to 1917 in the CLFD, inaccuracies and omissions are considerably greater in the earlier record, and the majority of provinces were not reporting in Canada until the 1960s and 1970s. Because of this, we restricted our analysis to 70 years postfire, which largely captures the change in albedo after fire and return to prefire conditions (Amiro et al., 2006; Randerson et al., 2006). In total, 49,215 fire events were analyzed with a total burned area of ~145 Mha (Figure 1), although the majority of recorded fires occurred after 1965 (Figure S1). We gridded the fire polygons to our MODIS 500 m grid using the 'raster' package (Hijmans et al., 2014) in R (R Core Team, 2012). To best avoid unburned pixel fractions, we used a fraction cover approach for regridding, and thereafter only considered pixels with 100% burn fraction in our analysis. We also excluded pixels that were designated as urban, crop, water, tundra, or temperate vegetation according to our land cover map.

2.2 | Blue sky albedo

We used satellite retrievals of albedo from MODIS as the target variable to train the random forest models. Currently available satellite products provide albedo modeled under the extreme and divergent conditions of pure diffuse illumination ('white sky' albedo) and pure direct illumination ('black sky' albedo). Albedo values are based on multiple, varied-angle measurements of surface reflectance and the RossThick-LiSparse Reciprocal (RTLSR) kernel-driven model with the Bidirectional Reflectance Distribution Function (BRDF) parameters retrieved for the target location and time. To accurately reflect ground illumination conditions, we created a daily 'blue sky' shortwave albedo product for every pixel and day in the study domain between 24 February 2000 (the first date available for MCD43A1) and 31 December 2017. 'Blue sky' refers to albedo under actual illumination conditions from a combination of both diffuse and direct illumination, and can be calculated using the RTLSR kernel equations with modified coefficients based on atmospheric and view-geometry conditions. At high latitudes, large solar zenith angles, and the presence of reflective snow- and ice-covered surfaces necessitate the consideration of multiple scattering events in the calculation of a more accurate blue sky albedo (Wang et al., 2012). Román et al. (2010) determined a set of optimal coefficients by using a radiative transfer model over a wide range of conditions for blue sky albedo calculations. The resulting lookup table provides quick access to the appropriate kernel coefficients based on snow cover, solar zenith angle, and aerosol optical depth (AOD) at 500 nm. These updated coefficients better account for increased anisotropic scattering which can occur under high AOD, high solar zenith angles, and/or snow-covered conditions, all of which are common at high latitudes.

To obtain the daily mean albedo, we calculated instantaneous blue sky albedo for each hour by estimating the solar zenith angle based on time, latitude, and day of the year. Hourly values were then weighted by their relative proportion of the total insolation over the whole day as described in Wang, Schaaf, Sun, Shuai, and Román (2018). Because BRDF and albedo calculations have been shown to have higher error at high solar zenith angles (Román et al., 2010), we used solar zenith angles over 70° only if no observation with a lower solar zenith angle was available, for example during the winter when the sun does not rise more than 20° above the horizon for large parts of our study domain. Because solar zenith angles above 70–74°

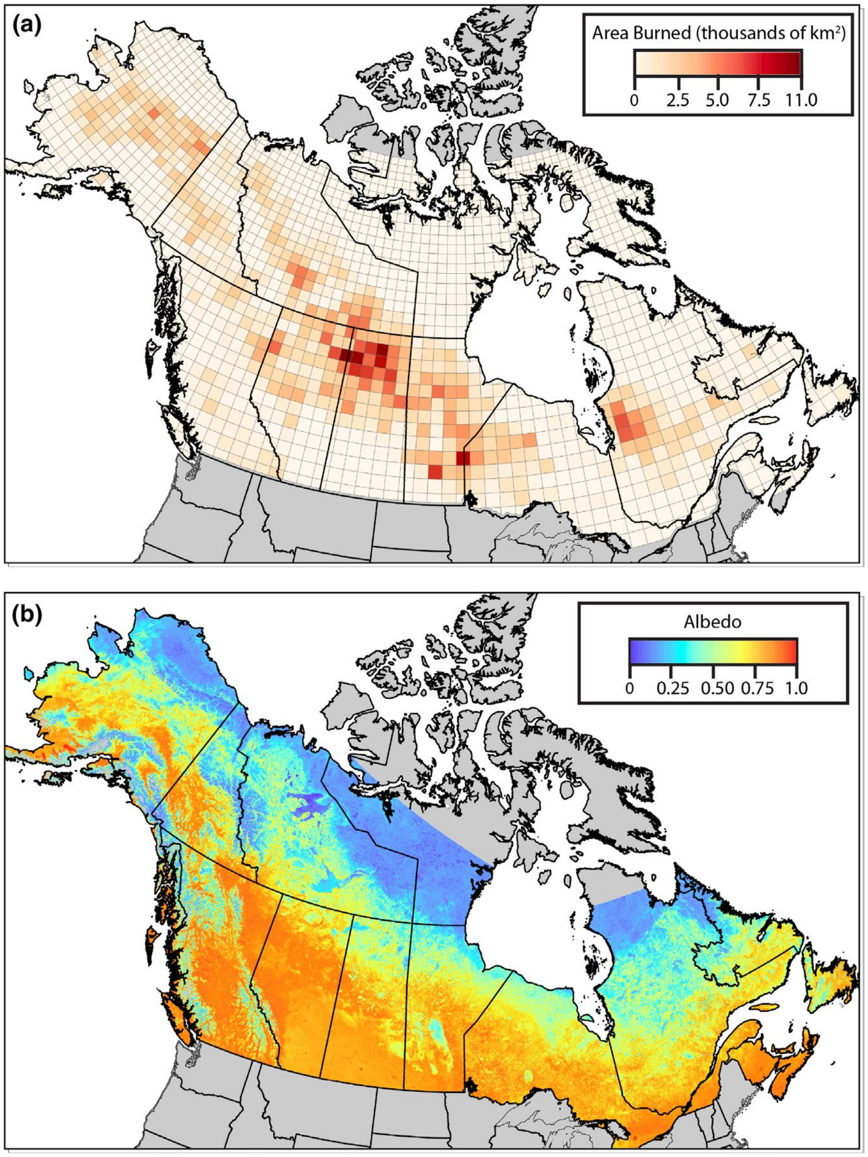

FIGURE 1 Fires included in our analysis, which ranged between 1930 and 2013, aggregated to 100 km grid cells (a), and mean blue sky albedo composite for the month of April during 2000–2013 (b). [Correction added on 17 December 2019 after first online publication: figures 1 and 4 have been updated in this current version.]

should be treated with extreme caution (Liu et al., 2009; Román et al., 2010), we also conducted two sensitivity analyses in which albedo observations were limited to (a) solar zenith angles <74° and (b) <70°. Although these sensitivity analyses utilized higher quality data in winter, they also limited data coverage (Section 2.7) and the available data was more heavily biased towards the southern boreal.

Daily BRDF model parameters were provided by the MODIS MCD43A1 V006 product (Schaaf & Wang, 2015; Wang et al., 2018). Solar insolation for each month was obtained from 3 hourly CERES SYN1deg top-of-atmosphere (TOA) fluxes (Wang et al., 2018), which we interpolated to hourly using a periodic spline and resampled to our 500 m grid. We used multiple sources for AOD estimates depending on availability. In descending order of preference, we used the MOD08 daily product (Platnick, Hubanks, Meyer, & King, 2015a), the MOD08 monthly product (Platnick, Hubanks, Meyer, & King, 2015b), the monthly Multi-angle Imaging SpectroRadiometer (MISR) MIL3MAE product (Diner, 2009) resampled to our MODIS 500 m grid, or the approximate global AOD mean of 0.2 (Yu et al., 2006) that is often assumed (e.g., Oh, Choi, Ho & Jeong, 2013; Wang, Liang, Schaaf & Strahler, 2010). The source of AOD for each pixel-date was recorded in the output quality flags, along with the presence or absence of snow, the quality flag from the MCD43A1 BRDF inputs, and whether or not the calculations included solar zenith angles greater than 70° (Solvik et al., 2019).

To model postfire albedo, we first filtered blue sky albedo by various quality flags in an effort to balance data quality versus quantity. For the months of May through September, when solar zenith angles are comparatively low, we included MCD43A1 pixels that were produced with full inversions of best or good quality (flags 0 or 1) and which had an AOD measurement derived from MOD08 or MISR. For all other months, in which data quality was generally poor, we included best or good quality MCD43A1 pixels without an AOD requirement. From these we created mean monthly composites for January through November (Figure 1). In December, due to large zenith angles, we did not directly calculate albedo. As mentioned above, we also conducted two sensitivity analyses in which albedo observations were required to have solar zenith angles <74° and <70°.

As a reference point for model results, we derived postfire albedo trajectories for each month using a retrogressive space-for-time approach, as has been commonly implemented (Beck et al., 2011; Lyons, Jin, & Randerson, 2008; Rogers et al., 2013). December trajectories were calculated as the average of November and January. We hypothesized that observed trajectories would contain systematic biases in later years compared to modeled trajectories. This is because some of the provinces contributing to the CNFD polygons did not begin reporting until the 1960s and early 1970s, thus biasing the observed trajectories to the southern boreal provinces of British Columbia, Alberta, Saskatchewan, and Manitoba roughly 40 years after fire (Figure S1). Previous findings have shown that the southern boreal has a lower albedo in nonsummer months compared to the northern boreal due to denser canopies and earlier snow melt, but a higher albedo in summer for several decades after a fire likely due to greater deciduous fractions (Jin et al., 2012). For illustrative purposes, we selected April and July as representative months for comparing spring and summer dynamics.

2.3 | Climate variables

Climate included historical data used to train the random forest model and future data used to project albedo for the 21st century. We acquired all climate variables from ClimateNA (Wang, Hamann, Spittlehouse, & Carroll, 2016; Table S1), which provides point estimates based on the coarse resolution Climate Research Unit (Mitchell & Jones, 2005) for the historical period and Climate Model Intercomparison Project 5 (CMIP5; Taylor et al., 2012) projections for the future. ClimateNA uses finder resolution PRISM (Daly, Gibson, Taylor, Johnson, & Pasteris, 2002; Daly et al., 2008) and ANUSLIN (Hutchinson, 1989) climate normals from 1961 to 1990 to downscale coarse-resolution monthly climate data to a 4 by 4 km grid, followed by bilinear interpolation and a locally derived elevation adjustment to estimate point data. Future climate data are harmonized with the historical time series using the delta method and a 1961–1990 baseline period. In our case, points represented the centroid of every burned pixel.

ClimateNA provides annual and seasonal historical variables for the years 1901–2013. We used annual data to assign climate during the year of fire (as a coarse proxy for fire weather conditions), and computed long-term climate means represented by the years 1971–2000 (indicative of average conditions for forest dynamics and succession). For seasonal variables, we considered only the spring (March–May) and summer (June–August) months. For future data, ClimateNA includes CMIP5 ensemble means from representative concentration pathways (RCPs) 4.5 and 8.5 (Meinshausen et al., 2011). Future projections are provided at three distinct epochs representing the mean during 30 year periods from (a) 2010 to 2039 (2020's), (b) 2040 to 2069 (2050's), and (c) 2070 to 2099 (2080's). To produce continuous long-term climate means for our modeling experiments (Section 2.7), we interpolated every variable between each epoch on an annual time step using a cubic spline, with 1971–2000 means (i.e., 1985) as the starting point.

The last climate variable we acquired was a permafrost zonation index (Gruber, 2012), which remained constant across climate scenarios. Although permafrost could be considered an environmental variable (see next section), we chose to include it here because the index is a function of mean annual air temperature.

2.4 | Environmental variables

We derived a number of environmental variables for model inputs including soil properties, topographic parameters, and permafrost zonation (Table S1). Soil properties were acquired from SoilGrids at a 250 m resolution (Hengl et al., 2017), including percent clay (0–2 µm), silt (2–50 µm), sand (50–2,000 µm), course material (>2,000 µm), bulk density (g/cm^3), soil organic carbon stock (tons/ha), soil organic carbon content (g/kg), soil water capacity until wilting point (volumetric fraction), and soil water pH. We integrated all variables across the top 30 cm of the soil profile.

For topographic variables, we used the Global Multi-resolution Terrain Elevation Data 2010 digital elevation model at 7.5 arc seconds (Danielson & Gesch, 2011; roughly 250 m) to derive elevation (m), aspect (°), and slope (°) for all burned pixels. We also calculated a topographic wetness index for each pixel that represents soil drainage patterns based on the slope and upslope area draining through a particular point (Beven & Kirkby, 1979). Lastly, we acquired a surface roughness index, which is a measure of how flat or mountainous the landscape is, from Gruber (2012). All inputs were regridded to the 500 m MODIS projection using bilinear interpolation.

We did not include other potentially important variables such as vegetation type and snow exposure, as these properties change over the course of succession and are therefore not independent predictors. Additionally, while fire severity, partly explained by the seasonal timing of fire (Turetsky et al., 2011), is an influential driver of postfire succession and therefore albedo (Beck et al., 2011), we excluded day of burn since it was not recorded for all fire records in the ALFD and CLFD and, when recorded, contained considerable uncertainty, especially in the earlier part of the record before the MODIS era.

To aid interpretation of our results and assess how soil type influenced species composition, we compared soil properties from SoilGrids that were found to be influential predictors of summer albedo (percent sand and silt) to a new deciduous fraction layer (Massey et al., 2019). Deciduous fraction for 2015 was initially mapped at 30 m and subsequently resampled to the SoilGrids 250 m grid using bilinear interpolation. We considered burned pixels based on the ALFD and CLFD between 1917 and 2013 (Section 2.1).

2.5 | Variable selection

Although random forests do not require collinear variables to be removed (Breiman, 2001), we employed a variable selection method to reduce computation time and facilitate interpretation, particularly regarding variable importance. We followed the methods of Kuhn and Johnson (2013), which involves the following iterative procedure: (a) calculate the correlation matrix of all variables, (b) determine the two predictors with the largest correlations, (c) remove the predictor from this set of two that has the largest mean correlation with all other variables, and (d) repeat until no two variables have a correlation above 0.7.

2.6 | Modeling postfire albedo

We tested several models to characterize monthly postfire albedo trajectories, including random forests, general additive models, boosted regression trees, and multivariate adaptive regression splines. In each case, models were initially implemented using year-since-fire as a predictor. However, by comparing output to our observed chronosequences, we determined that no model was capable of capturing the full influence of year-since-fire, particularly in the winter and spring when variance in albedo was influenced by several predictors more important than year-since-fire (Figure S2). Because of this, and the fact that our data volume was not limiting, we built separate monthly models for each year-since-fire, and subsequently smoothed the resulting trajectories using a general additive model with six splines. Due to the relatively poor quality in fire records further back in the historical record, and because modeled postfire albedo generally retained its prefire values after roughly 70 years, we evaluated albedo up until 70 years postfire.

Once collinear variables were removed, all remaining variables were used to train the suite of models. Each model was cross-validated by training on 80% of the data and testing on 20%. Sample sizes were variable depending on month and year-since-fire, with a minimum of 7,500 and a mean of 398,000 pixels across all months and years. When cross-validated R^2 values were compared between model versions, random forest was the most accurate and therefore selected as our primary approach. We built random forest models using the h2o package in python (H2O.ai, 2016) with 50 trees, a maximum of 20 splits per tree, and p/3 number of predictors when searching for the best split where p is the total number of predictors. Model results were interpreted for each month using feature importance and partial dependence plots. Feature importance was calculated by the improvement in mean square error averaged across all trees for respective variables, whereas the partial dependence accounts for a given variable's marginal effects after averaging the effects of all others. For simplicity, and to be able to assess the importance of year-since-fire as a driver, we report feature importance for each monthly albedo trajectory using the model version that included year-since-fire as a predictor (as opposed to the 70 separate models for each year which were used for other analyses). When model fits are presented with R^2 values, these represent the mean testing set R^2 across all 70 model years for a given month.

2.7 | Postfire albedo predictions

Our aim was to predict postfire albedo under mean historical and future climate conditions (RCP 4.5 and 8.5). To do so, we applied our models to a random sample of 10,000 pixels that burned in the MODIS era (between 2003 and 2013). Because we typically had fewer available albedo observations in nonsummer months in the northern part of our domain, we weighted our sampling distribution by the percentage of historical burned pixels within a broad 700 km grid in order to ensure relative spatial representativeness. Despite this large grid, data were still sparse at high latitudes in the winter months. For example, we were only able to use 4,400 and 4,700 pixels in our main analysis during the months of November and January, respectively; 1,744 and 876 pixels in our sensitivity analysis excluding solar zenith angles over 74°; and 458 and 91 pixels in our sensitivity analysis excluding solar zenith angles over 70°. We chose 2003 as the lower limit so that at least 2 years of prefire albedo data would be available for our forcings analysis (Section 2.8). The year 2013 was chosen as the upper limit because it corresponds to the end of the historical climate record available from ClimateNA.

For the purposes of spatial representativeness when comparing modeled trajectories to observed chronosequences, we also modeled a separate sample of 10,000 pixels across the entire fire record (Figures S5 and S7). For future scenarios, all environmental and year-of-burn climate variables were kept at their historic values, but the long-term climate variables changed annually (Table S1). All fires from the 10,000 MODIS-era pixels were experimentally burned in the year 2016, and albedo was predicted 70 years postfire (corresponding to 2085 in the future scenarios). We thus present three scenarios: (a) fires burning in 2016 and climate remaining at historical conditions thereafter ('historical'), (b) fires burning in 2016 and climate changing according to RCP 4.5, and (c) fires burning in 2016 and climate changing according to RCP 8.5. Year-of-fire variables were always derived from the actual observed fire years in order to avoid misrepresenting fire weather conditions. Model output is presented at an aggregated 100 km grid for ease of interpretation (Figure 1).

2.8 | Conversion to radiative forcing

To convert our modeled changes in albedo from the sample of 10,000 pixels into RF, we used previously derived linear radiative kernels that represent changes in TOA forcing per unit change in land surface albedo, similar to previous work (Chen, Liang, & Cao, 2016; O'Halloran et al., 2012, 2014). We selected albedo-specific radiative kernels from Shell et al. (2008), which are provided at their native 2.5° resolution (from the Community Atmosphere Model version 3; Collins et al., 2006) for each month, and were resampled to our spatial model grid (100 km; Figure 1) using bilinear interpolation. We calculated RF by taking the difference between each pixel's postfire albedo and prefire albedo (based on all available prefire observations for each month, with a minimum of one observation) for each postfire year and month, and then applied the appropriate kernel based on spatial location. Monthly RF trajectories were calculated as well as the annual mean.

2.9 | Uncertainty

One limitation with the majority of statistical modeling techniques, including random forests, is they are unable to extrapolate beyond the range of inputs used for model training. Despite this limitation, we chose a random forest due to its superior performance compared to other models, as assessed by cross-validated R^2 values, and because all models tested would have been limited by extrapolation uncertainty. For the RCP 4.5 and 8.5 scenarios, there are numerous pixels where future climate variables exceeded the historical range of variability. When this occurred, the random forest predicted, for any particular variable, the average value across all trees in the forest found at the first decision split. In our case, due to the relationship between albedo and mean maximum summer surface air temperature, this occurred near the upper end of the temperature range and corresponded to 26.73°C, or the 99.99th percentile. Hence, any pixel which experienced a future climate value above this threshold at some point was considered to be 'Outside Range', after which the random forest models were relatively insensitive to changing climate. To evaluate how this influenced our RF estimations, we compared predictions across three sets of pixels: (a) all 10,000 pixels ('All'), (b) those pixels for which climate did not exceed the historical range of variability for an influential representative climate variable (mean maximum summer surface air temperature) and month (April; termed 'Within Range'), and (c) only those pixels for which climate did exceed the historic range of variability (Outside Range), for both RCP 4.5 and 8.5. We present the range of RFs between the All and Within Range sets of pixels for each RCP scenario as lower and upper bounds, respectively, as an estimate of overall uncertainty. This tends to be a conservative range since the set of All pixels includes Outside Range pixels, which at some point have lost sensitivity to changing climate.

We also include a separate measure of model uncertainty as indicated by the cross-validated testing set root mean square error (RMSE). When results are expressed on a monthly basis, RMSE represents the mean across all model years, and when results are expressed annually, RMSE is expressed as the mean across all months.

3 | RESULTS

Random forest models displayed strong fits to the observational data ($R^2 > .80$; Figure 2). There was, however, variation between seasons, likely related to differences in the types of predictor variables that influenced albedo and thereby the strength of those relationships (Figure S2). In spring (represented by April), the most influential variables were related to permafrost and temperature, presumably via their influence on snow cover dynamics and canopy density (Figure S3).

As expected, warmer temperatures and lower permafrost indices resulted in lower spring albedo. In summer months (represented by July), soil characteristics were more important, presumably due to their influence on nutrient cycling, soil moisture, and therefore tree species and successional dynamics. Partial dependence plots (Figure S3) indicated that siltier soils had higher summer albedo and sandier soils had lower summer albedo. This is likely related to the increased reflectance of deciduous broadleaf species and their competitive advantage on silty soils, and is corroborated by the relationships between percent sand and silt to deciduous vegetation (Figure S4): deciduous fraction generally increased as soils became siltier, and decreased as soils became sandier. Although we found three variables related to soil highly influential in the summer (% coarse, sand and silt), we also found that when these variables were recursively eliminated from the model, no single soil property improved model accuracy more than another, and that model fits as evaluated by R^2 were relatively unchanged as long as any one of the three soil properties were included. When included, year-since-fire was much more important for summer months than for spring, highlighting the importance of species composition and its determinants for summer albedo, as well as the large variability in spring albedo and its climatic drivers across Alaska and Canada (e.g., Figure 1).

Although modeled albedo matched observations well for any given month and year-since-fire, when these models were applied to our random subset of 10,000 pixels across the fire record, the predicted trajectory diverged from the observation-derived chronosequence substantially after roughly 40 years (Figure S5). Consistent with our original hypothesis, there is strong evidence to suggest this is due to the spatial biases in reported fires in the early ALFD and CNFD fire records, which are heavily dominated by the Canadian southern boreal provinces before ~1965. This bias can be seen clearly in Figure S1 through patterns of burned area, and in terms of nonstationarity in the influential inputs over time. For example, the mean inputs of permafrost index, mean maximum spring temperature, and soil organic carbon stocks for the observed chronosequence of fire pixels show deviations after roughly 40 years since fire, corresponding to a greater contribution from the warmer southern boreal provinces and hence lower albedo (Figure S6). This was further corroborated by an experiment in which random forest models from specific years-since-fire were applied to inputs from all other years, again showing consistent trends after roughly 40 years since fire (Figure S7).

Under historical climate, we estimated that fires led to an annual cooling of -1.77 ± 1.36 W/m^2 for the first 70 years after fire, but there was substantial and expected variation in predicted historical albedo and RF between months based on our sample of 10,000 pixels during the MODIS era (Figure 3). Winter and spring months showed much larger modeled albedo than summer and fall months, and thereby contributed a more negative RF even after accounting for lower solar insolation (via monthly radiative kernels). For instance, the mean cumulative monthly RF integrated 70 post-fire years was -5.64 ± 3.27 and -5.42 ± 3.75 W/m^2 for March and April, respectively, while in July and August the mean cumulative RF was -1.08 ± 0.83 and -0.92 ± 0.72 W/m^2. When albedo observations with solar zenith angles above 74° and 70° were excluded (our two sensitivity analyses), mean cumulative RF was -2.07 ± 1.36 and -2.21 ± 1.36 W/m^2, respectively.

Under the RCP 4.5 scenario, our models displayed an increase (warming effect) of 0.27 W/m^2, or a 15% increase compared to historical climate. Using solar zenith angles below 74° and 70°, we estimated a mean RF increase of 0.28 W/m^2 (14%) and 0.25 W/m^2 (11%), respectively. Seasonally, there was also notable variation for future

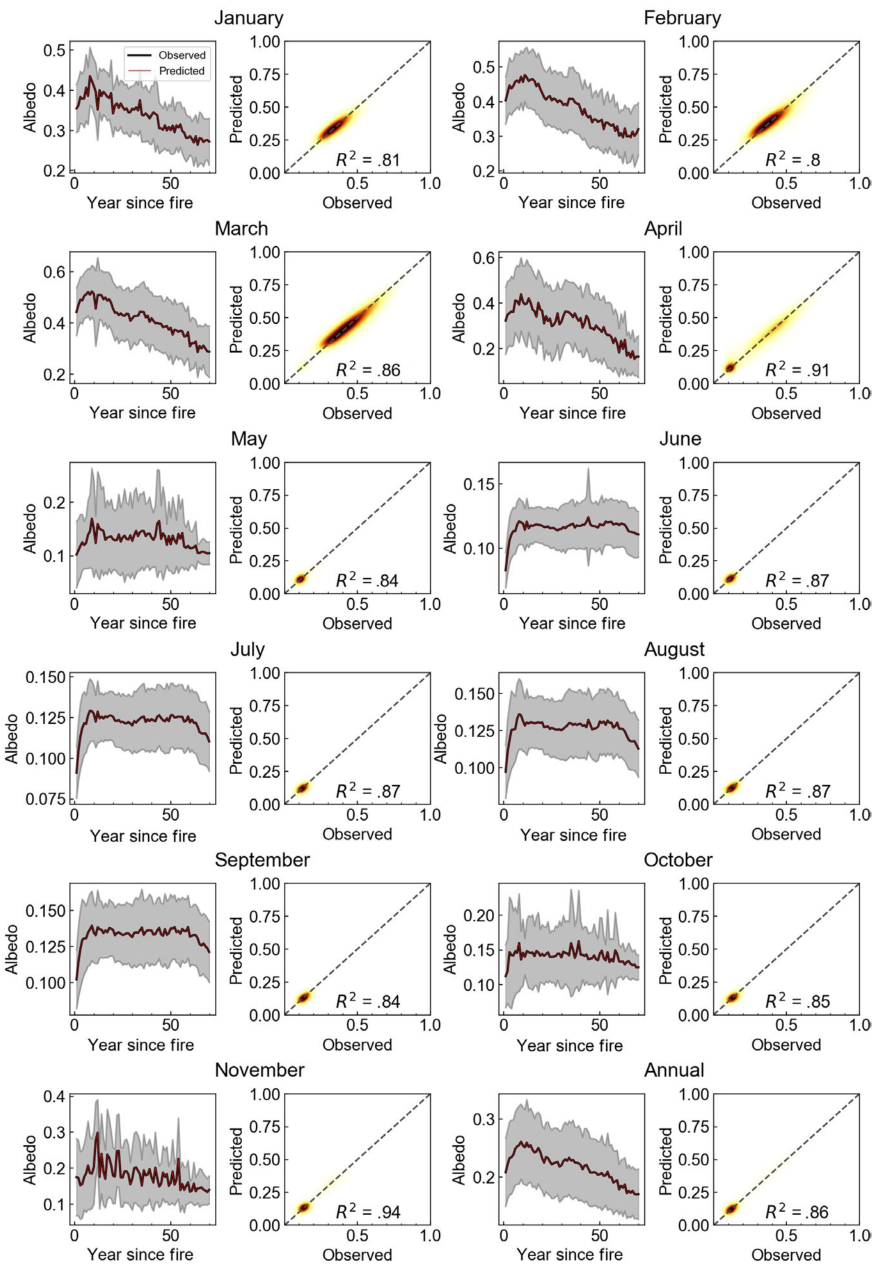

FIGURE 2 Mean observed post-fire albedo compared to mean predicted albedo for each month and post-fire year (left panels), and density plots of observed vs predicted values and associated R^2 (right panels). R^2 are based on fits from the test set during cross-validation. Note that December was not modeled directly and therefore not included here, and that the aggregated annual mean albedo is presented in the bottom right. Grey shading represents the standard deviation of predicted pixels

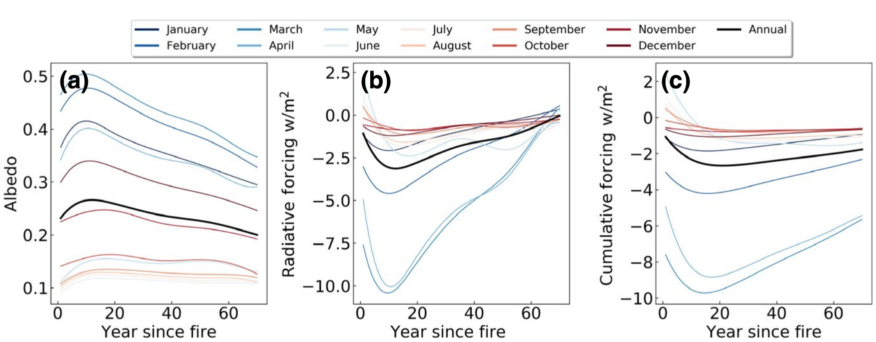

FIGURE 3 Monthly and annual modeled post-fire albedo (a), radiative forcing (b) and cumulative mean forcing (c) for a sample of 10,000 pixels that burned in the MODIS era (2003–2013). For each pixel, we calculated a pre-fire control value based on available observations (at least 2 years) that was used to determine post-fire radiative forcing

climate scenarios. Our models displayed a substantial reduction in spring albedos under future climate and a minor increase in summer months (RCP 4.5 shown in Figure 4a,c). Mean annual RF for the RCP 4.5 scenarios was −4.59 ± 3.23 W/m^2 (19% increase from historical climate) in March and −3.41 ± 3.61 W/m^2 (37% increase) in April, while in July and August mean RF was −1.23 ± 0.84 W/m^2 (12% decrease) and −1.06 ± 0.73 W/m^2 (13% decrease), respectively. These patterns are indicative of warmer climates leading to decreases in

FIGURE 4 Comparison of predicted post-fire albedo trajectories for historical, RCP 4.5, and RCP 8.5 climates employing transient (a, c) and equilibrium (b, d) scenarios for the representative months of April (a, b) and July (c, d). Equilibrium scenarios use mean climate centered around three thirty-year time periods (2025, 2055, and 2085). [Correction added on 17 December 2019 after first online publication: figures 1 and 4 have been updated in this current version.]

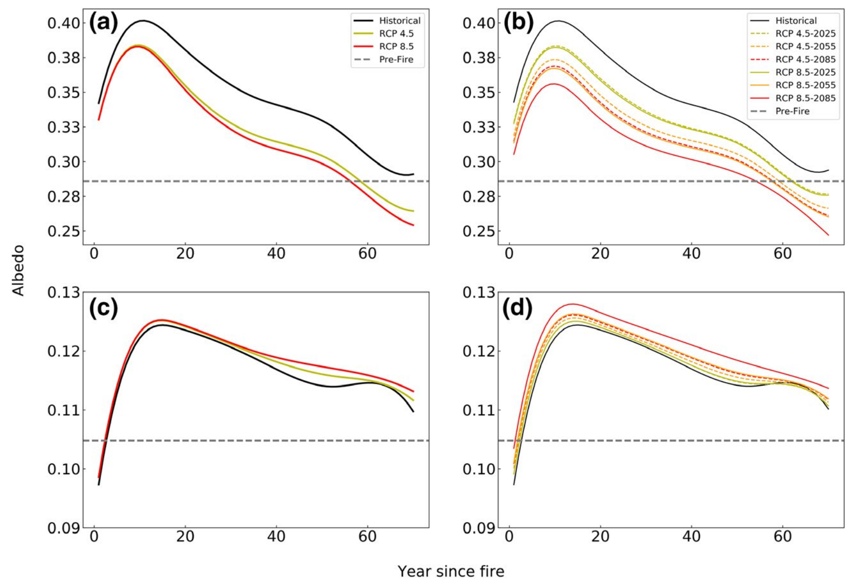

FIGURE 5 Mean annual albedo (a), radiative kernels (b), and radiative forcing (c) based on historical climate

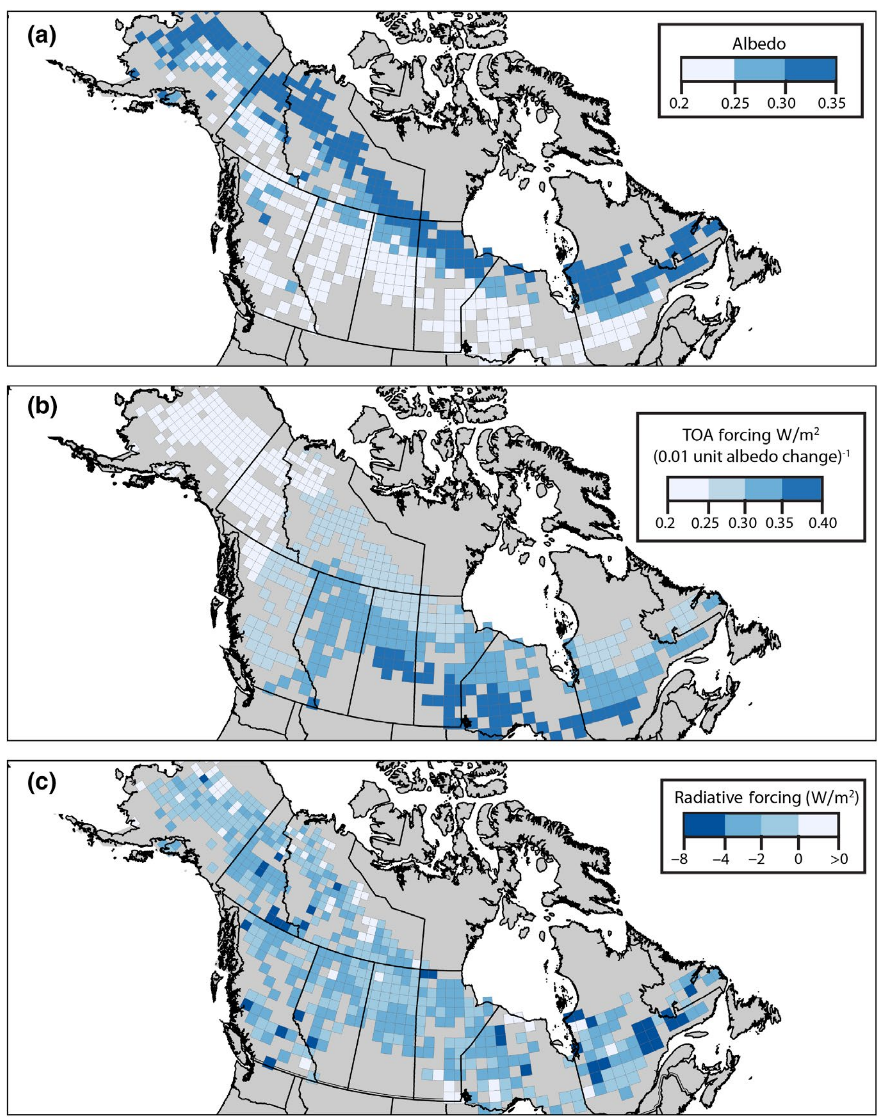

snow extent during the spring, and more reflective summer successional trajectories presumably due to greater deciduous fractions.

Surprisingly, the differences in albedo and RF between the historical and RCP 4.5 scenarios were substantially greater than that between RCP 4.5 and 8.5 (Figure 4a,c). The reasons for this were twofold: (a) our experimental setup and (b) future climate conditions that went outside the range of historic variability. To examine the influence of our experimental setup (a), we conducted additional simulations in which the long-term future climates came from the three 'equilibrium' scenarios (i.e., 2020s, 2050s, and 2080s), as opposed to being interpolated on an annual time step. Results showed that the two RCP scenarios did not diverge in a substantial way until the latter half of the 21st century (2080s; Figure 4b,d). However, regardless of time epoch, the largest differences from historical trajectories were seen in the early decades after fire, whereas scenarios converged more during canopy closure in later succession. Because our experimental setup used transient climate changes, differences between the RCP scenarios only began to appear in a substantial way toward the end of the time series, and were dampened by the co-occurring late successional stages. This also suggests that fires burning later in the 21st century would show more immediate divergence between the two RCP scenarios.

Perhaps more importantly, the two RCP scenarios displayed large differences in the fraction of pixels that were considered Outside Range (i.e., climate inputs went outside the historic range of variability): 25% for RCP 4.5 and 41% for RCP 8.5. As long-term mean climate continued to warm during the 21st century, so did the likelihood that it obtained values beyond what was observed historically for the domain. When this occurred, which happened more frequently in the southern boreal (Figures S8 and S9) and under the more severe RCP 8.5 scenario, our random forest models were unable to account for the influence of further climate changes. As a result, the trajectories for Outside Range pixels had lower albedo and smaller differences compared to historical versus Within Range pixels (Figure S8). Using the All and Within Range sets of pixels as lower and upper bound estimates, we estimate an increase of 0.27–0.28 W/m^2 (15%–16% reduction in negative forcing) under RCP 4.5 and 0.41–0.49 W/m^2 (23%–28% reduction in negative forcing) under RCP 8.5.

In terms of spatial patterns, there was considerable large-scale variation in mean annual postfire albedo (Figure 5a), with the northern (largely unmanaged) boreal showing larger albedos over the course of postfire succession. However, because radiative kernels showed nearly opposite trends (Figure 5b), primarily a function of latitudinal gradients in annual insolation, overall mean RF displayed minimal large-scale spatial patterns (Figure 5c).

Nonetheless, we found that eastern Canada and parts of the Canadian Rockies tended to contain the largest negative RFs because of their relatively cold climates and thus high postfire albedos compared to their latitudinal position. This is due to large-scale climate gradients (i.e., polar jet stream position) in the case of eastern Canada, and high-elevation forests in the case of the Canadian Rockies. A small number of pixels (3.5%) exhibited a positive forcing (Figure 5c), but this tended to occur when only one or two prefire observations were available. Future changes in RF for both RCP 4.5 and 8.5 showed somewhat consistent patterns of greater differences in the northern domain, particularly within central and eastern Canada (Figure S10). Nevertheless, it is difficult to distinguish true spatial patterns from those induced by Outside Range pixels (i.e., pixels in which climate influences saturated), as these were concentrated in the southern boreal and covered a majority of the domain for RCP 8.5 (Figure S9).

4 | DISCUSSION

Our study follows a rich history of investigations regarding the influence of North American boreal forests and fires on surface energy budgets and climate (e.g., Bright et al., 2017; Chapin et al., 2000; Randerson et al., 2006; Shugart, Leemans, & Bonan, 1992). These forests exhibit a rather unique regime of almost exclusively high-intensity crown fires (Wooster & Zhang, 2004), leading to relatively large impacts on albedo (Rogers et al., 2015). Our approach is unique in that we developed data-driven statistical models of postfire albedo, as opposed to relying purely on observed chronosequences. This allowed us to provide insights into the major spatial drivers of postfire albedo and to make projections under future climate scenarios. Our models showed the distinct influence of climate patterns on winter and spring albedo (through their influence on canopy cover and snow exposure), and year-since-fire and soil properties on summer albedo (through their influence on species composition). Late winter and spring albedo is most important from a climate forcing perspective (Figure 3; Rogers et al., 2013), which is why our models estimated substantial reductions in the overall cooling effect from fires (15%–28%) due to warmer springs and therefore less spring snow cover and lower albedo in future climate scenarios.

Our models of postfire albedo generally agree with previous findings using observed chronosequences, which supports our applications of these models. Summer albedo decreases during the first 1–3 years after fire from charred surfaces and the deposition of black carbon, but then increases as vegetation re-establishes. The largest increases in albedo are in the spring and winter months due to increased snow exposure. Our trajectories and change from prefire are comparable to past studies using MODIS albedo (Jin et al., 2012; Lyons et al., 2008; Rogers et al., 2015), but are also lower (Liu & Randerson, 2008) and higher (Amiro et al., 2006) than field-based chronosequences. These differences are likely related to variability in the spatial gradients in postfire albedo (Figure 5a), the domain of each study (e.g., Alaska vs. all of boreal North America), the presence of unburned patches and nonforest fractions within 500 m MODIS pixels, relatively poor-quality fire polygons early in the ALFD and CNFD records, the method used to estimate prefire control values, and illumination conditions of the albedo products (black sky, white sky, or blue sky; Figure S11). Regarding the latter, we developed a blue sky albedo product to represent the influence of multiple scattering, which can be significant for snow covered surfaces and high zenith angles, and therefore important when assessing albedo dynamics in high latitude environments (Román et al., 2010; Wang et al., 2012, 2014).

As demonstrated by Lyons et al. (2008), the method used to estimate prefire control values may be particularly important for assessments of the albedo-induced RF, as the albedo from unburned pixels selected as controls (typically mature conifer forests) may not match prefire observations. To facilitate comparisons between studies, we use the assumption that RF is roughly 60% of Surface Shortwave Forcing (SSF; Randerson et al., 2006). Using this conversion, Lyons et al. (2008) reported a mean annual RF of −3.72 W/m^2 for 50 years after fire in interior Alaska when using unburned evergreen pixels as control, and −1.8 W/m^2 when using prefire observations. Our experimental setup also uses prefire observations as control, and finds an annual RF of −2.19 ± 1.37 W/m^2 during the first 50 years after fire across the domain, and −1.44 ± 1.37 W/m^2 just within interior Alaska. Our estimates are also similar to Jin et al. (2012), who reported a mean annual RF of −2.5 ± 0.2 W/m^2 for the initial 30 years after fire in central Canada using prefire observations as a control. Our models estimated −2.58 ± 1.42 W/m^2 during the first 30 years after fire across the domain, and −2.25 ± 1.42 W/m^2 within Jin et al.'s central Canadian study domain.

Nonetheless, our RF estimates are significantly lower in magnitude compared to studies using field-based albedo and unburned conifer forests as controls. ALthough Randerson et al. (2006) reported a mean annual RF of −4.2 ± 2.0 W/m^2 for 80 years postfire in interior Alaska, and O'Halloran et al. (2012) reported −4.5 W/m^2 for 70 years postfire in Manitoba, our models suggest a mean annual forcing of −1.77 ± 1.36 W/m^2 for 70 years postfire across the domain, −1.08 ± 1.36 W/m^2 in interior Alaska, and −2.08 ± 1.36 W/m^2 in Manitoba. In addition to the potential discrepancies mentioned above, these comparisons in particular may highlight differences arising from the different methods used to estimate RF from SSF. One other important consideration was that we found space-for-time albedo chronosequences derived from the ALFD and CNFD fire records to be biased due to the changing spatial distribution of reported fires through time. In particular, the dominant influence of the Canadian southern boreal provinces before the mid-1960s tended to bias postfire albedo in the later decades of succession (after roughly 40 years) toward lower albedos in the influential spring months due to higher canopy densities and lower snow exposure. Depending on the spatial domain considered, this may amplify the range of postfire albedo values observed using the traditional chronosequence approach. We suggest this phenomenon should be considered in future studies using the large fire databases to derive postfire trajectories, such as we do here by using statistical models.

In terms of overall spatial patterns, our results show a distinct latitudinal-climatic gradient in postfire albedo that increases from south to north (Figure 5a). However, due to the nearly opposite trend in solar insolation and hence TOA radiative kernels (Figure 5b), the resulting postfire annual RF displayed no distinct spatial patterns at a broad scale (100 km; Figure 5c). This has implications for other large-scale modeling efforts, and potentially management and policy decisions aimed at climate mitigation. This result is also supported by Jin et al. (2012), who found no latitudinal trends in SSF on an annual basis within central Canada due to opposing north–south gradients in albedo and solar insolation.

Although we found no distinct large-scale spatial patterns in postfire albedo RF, our comparison of climate scenarios clearly demonstrated a reduction in albedo during the course of postfire succession in the future. This led to a 15%–28% reduction in the cooling impact from fires, primarily due to warming in the spring and consequent reductions in snow cover, a pattern that is already playing out across the arctic–boreal region (Atlaskina et al., 2015; Chen, Loboda, He, Zhang, & Liang, 2018; Chen et al., 2016; Li et al., 2018). Although we did not include historical or future snow cover extent as an explicit predictor variable, our random forest models were able to capture the relationships between climate variables and the influence of snow cover. This finding is consistent with Euskirchen et al. (2016), who projected a reduction in albedo across Alaska and northwest Canada due to a decrease in snow duration, despite a cooling effect from brighter vegetation as a result of increased burning. While not directly estimating changes in RF, our findings are similar to Bright et al. (2014), who found that April albedo in Norwegian boreal forests decreased by 16%–24% under RCP 4.5 and 8.5 scenarios, respectively.

Although we quantified uncertainty in our model predictions, there are still a number of sources of uncertainty and caveats that should be considered when interpreting our results. Firstly, our results strongly suggest that historical postfire albedo chronosequences are biased low after roughly 40 years postfire due to inconsistent spatial and temporal fire records in the ALFD and CLFD. This leads to difficulties in a statistical framework because the observed data drives the model, and thus propagates into predictions. Although our model results are arguably able to predict the correct range of albedos despite the biased observational distribution (Figures S5 and S7), we have no definitive way of examining the impact on our overall results. Secondly, random forest models are not well suited to extrapolate beyond the range of input conditions experienced by the training data. When this occurs for any tree-based model, predictions will represent the largest (or smallest) value associated with a particular variable in the training set. Hence, we believe our future projections are relatively conservative, although we did present results for the subset of pixels in which future climate did not extend beyond the historical range as upper bounds. Nevertheless, this difficulty that statistical models have with extrapolation suggests that using a mechanistic model may be fruitful. Our study also suffers from the common issue of unburned islands contained in historic fire perimeters, which have been estimated to cover roughly 10%–20% of burned polygons (Kolden, Lutz, Key, Kane, & van Wagtendonk, 2012; Rogers et al., 2014; Sedano & Randerson, 2014; Veraverbeke et al., 2015). Our modeled trajectories therefore arguably underestimate postfire albedo to the same magnitude, although this bias likely changes as a function of year-since-fire. Regarding our albedo data, acquiring satellite observations in high latitudes is difficult due to low solar zenith angles and high albedos in the nonsummer seasons. To address this, we assessed how our results changed when restricting observations to have solar zenith angles less than 74° and 70°, finding that historical forcing decreased slightly (became more negative). Regardless, we did not find notable differences in the warming effect when future RCP scenarios were compared. We also recognize that the MODIS 500 m grid may in fact reflect a somewhat larger area (Campagnolo et al., 2016), which could lead to underestimates of postfire albedo due to the influence of unburned forest patches. In addition, albedo may be underestimated as remaining structural elements in the landscape (e.g., snags and surviving trees) could be disproportionately considered by the algorithm. This is corroborated by modeling studies over forested areas which found that the effective spatial resolution of the albedo product is strongly linked with forest structure (Hovi, Lindberg, & Lang, 2019). There is also uncertainty in the radiative kernels used to derive RF due to nonlinearities in the albedo feedback (Shell et al., 2008), which may change in the future due to altered cloud properties. Lastly, unlike process models, statistical models are unable to account for dynamic processes that may change in the future such as shifting vegetation distributions, CO_2 fertilization, nutrient cycling, and permafrost loss, all of which either directly or indirectly influence postfire albedo and overall RF.

Despite these limitations, our study represents a significant advance in being able to understand, model, and project fire impacts across boreal North America under a changing climate. Our approach and results have the potential to improve land and Earth system models, for example by providing validation data for the influence of forest structure and plant functional type composition during postfire recovery on modeled albedo. These models currently lack robust representations of fire effects in boreal environments and contain significant biases in albedo parameterizations (Li et al., 2016; Loranty, Berner, Goetz, Jin, & Randerson, 2014). Our approach also has the potential to inform land management. Fire managers have some level of control over fire behavior and extent, currently spending hundreds of millions to billions of dollars (US$) per year in fire suppression across Alaska and Canada (Melvin et al., 2017; Stocks & Martell, 2016). The warming or cooling influence of forest fires is not currently accounted for, but could be useful for targeted management and suppression activities focused on climate impacts, given adequate information, policy frameworks, and resources. Fine-scale information on climate forcings from wildfires, such as albedo, greenhouse gas, and aerosol emissions, could help inform such decisions.

We recommend that future work further refines our approach and explores broader implications. For example, spatial dynamics and heterogeneity could be advanced by using higher resolution imagery for albedo and historical burned areas, such as from Landsat and Sentinel-2 (Kuusinen, Tomppo, Shuai, & Berninger, 2014; Li et al., 2018; Wang, Erb, et al., 2016). We also recommend investigations at landscape scales, for which modeled postfire albedo for any given pixel could be constrained by postfire observations. The negative forcings from albedo should also be compared to those from emitted greenhouse gasses and aerosols to better understand spatial and seasonal controls on net climate forcing from boreal forest fires, as well as how all these forcings will be altered by climate change and evolving fire regimes.

ACKNOWLEDGEMENTS

This work was funded by the National Aeronautics and Space Administration (NASA) Arctic-Boreal Vulnerability Experiment (ABoVE; NNX15AU56A). The MODIS albedo products are supported by NASA NNX14AI73G. Our analysis would not have been possible without open access to long-term fire records in Alaska and Canada, high-quality observations from the MODIS instruments, and customizable climate data from ClimateNA.

ORCID

Stefano Potter https://orcid.org/0000-0002-5141-3409
Jill F. Johnstone https://orcid.org/0000-0001-6131-9339
Xanthe J. Walker https://orcid.org/0000-0002-2448-691X
Brendan M. Rogers https://orcid.org/0000-0001-6711-8466

REFERENCES

Abis, B., & Brovkin, V. (2017). Environmental conditions for alternative tree-cover states in high latitudes. *Biogeosciences*, *14*(3), 511–527. https://doi.org/10.5194/bg-14-511-2017

Alexander, H. D., & Mack, M. C. (2016). A canopy shift in interior Alaskan boreal forests: Consequences for above- and belowground carbon and nitrogen pools during post-fire succession. *Ecosystems*, *19*(1), 98–114. https://doi.org/10.1007/s10021-015-9920-7

Amiro, B. D., Barr, A. G., Barr, J. G., Black, T. A., Bracho, R., Brown, M., … Xiao, J. (2010). Ecosystem carbon dioxide fluxes after disturbance in forests of North America. *Journal of Geophysical Research*, *115*, https://doi.org/10.1029/2010JG001390

Amiro, B. D., Orchansky, A. L., Barr, A. G., Black, T. A., Chambers, S. D., Chapin III, F. S., … Randerson, J. T. (2006). The effect of post-fire stand age on the boreal forest energy balance. *Agricultural and Forest Meteorology*, *140*(1–4), 41–50. https://doi.org/10.1016/j.agrformet.2006.02.014

Amiro, B. D., Todd, J. B., Wotton, B. M., Logan, K. A., Flannigan, M. D., Stocks, B. J., … Hirsch, K. G. (2001). Direct carbon emissions from Canadian forest fires, 1959–1999. *Canadian Journal of Forest Research*, *31*(3), 512–525. https://doi.org/10.1139/cjfr-31-3-512

Atlaskina, K., Berninger, F., & de Leeuw, G. (2015). Satellite observations of changes in snow-covered land surface albedo during spring in the Northern Hemisphere. *The Cryosphere*, *9*(5), 1879–1893. https://doi.org/10.5194/tc-9-1879-2015

Balshi, M. S., McGuire, A. D., Duffy, P., Flannigan, M., Walsh, J., & Melillo, J. (2009a). Assessing the response of area burned to changing climate in western boreal North America using a Multivariate Adaptive Regression Splines (MARS) approach. *Global Change Biology*, *15*(3), 578–600. https://doi.org/10.1111/j.1365-2486.2008.01679.x

Balshi, M. S., Mcguire, A. D., Duffy, P., Flannigan, M., Kicklighter, D. W., & Melillo, J. (2009b). Vulnerability of carbon storage in North American boreal forests to wildfires during the 21st century. *Global Change Biology*, *15*(6), 1491–1510. https://doi.org/10.1111/j.1365-2486.2009.01877.x

Beck, P. S. A., Goetz, S. J., Mack, M. C., Alexander, H. D., Jin, Y., Randerson, J. T., & Loranty, M. M. (2011). The impacts and implications of an intensifying fire regime on Alaskan boreal forest composition and albedo. *Global Change Biology*, *17*(9), 2853–2866. https://doi.org/10.1111/j.1365-2486.2011.02412.x

Beven, K. J., & Kirkby, M. J. (1979). A physically based, variable contributing area model of basin hydrology. *Hydrological Sciences Bulletin*, *24*(1), 43–69. https://doi.org/10.1080/02626667909491834

Bonan, G. B., Pollard, D., & Thompson, S. L. (1992). Effects of boreal forest vegetation on global climate. *Nature*, *359*(6397), 716–718. https://doi.org/10.1038/359716a0

Bond-Lamberty, B., Peckham, S. D., Ahl, D. E., & Gower, S. T. (2007). Fire as the dominant driver of central Canadian boreal forest carbon balance. *Nature*, *450*(7166), 89–92. https://doi.org/10.1038/nature06272

Boulanger, Y., Parisien, M.-A., & Wang, X. (2018). Model-specification uncertainty in future area burned by wildfires in Canada. *International Journal of Wildland Fire*, *27*(3), 164–175. https://doi.org/10.1071/WF17123

Breiman, L. (2001). Random forests. *Machine Learning*, *45*(1), 5–32. https://doi.org/10.1023/A:1010933404324

Bright, R. M., Antón-Fernández, C., Astrup, R., Cherubini, F., Kvalevåg, M., & Strømman, A. H. (2014). Climate change implications of shifting forest management strategy in a boreal forest ecosystem of Norway. *Global Change Biology*, *20*(2), 607–621. https://doi.org/10.1111/gcb.12451

Bright, R. M., Davin, E., O'Halloran, T., Pongratz, J., Zhao, K., & Cescatti, A. (2017). Local temperature response to land cover and management change driven by non-radiative processes. *Nature Climate Change*, *7*(4), 296–302. https://doi.org/10.1038/nclimate3250

Brown, C. D., & Johnstone, J. F. (2012). Once burned, twice shy: Repeat fires reduce seed availability and alter substrate constraints on Picea mariana regeneration. *Forest Ecology and Management*, *266*, 34–41. https://doi.org/10.1016/j.foreco.2011.11.006

Brown, D. R. N., Jorgenson, M. T., Kielland, K., Verbyla, D. L., Prakash, A., & Koch, J. C. (2016). landscape effects of wildfire on permafrost distribution in interior Alaska derived from remote sensing. *Remote Sensing*, *8*(8), 654. https://doi.org/10.3390/rs8080654

Campagnolo, M. L., Sun, Q., Liu, Y., Schaaf, C., Wang, Z., & Román, M. O. (2016). Estimating the effective spatial resolution of the operational BRDF, albedo, and nadir reflectance products from MODIS and VIIRS. *Remote Sensing of Environment*, *175*, 52–64. https://doi.org/10.1016/j.rse.2015.12.033

Canada Centre for Remote Sensing (CCRS). (2013). *2005 Land cover of North America at 250 meters, Version 2.0*. Earth Sciences Sector, Natural Resources Canada. Retrieved from http://www.cec.org/naatlas/

CAVM Team. (2003). *Circumpolar arctic vegetation map*. Retrieved from https://www.geobotany.uaf.edu/cavm/

Chambers, S. D., & Chapin, F. S. (2002). Fire effects on surface-atmosphere energy exchange in Alaskan black spruce ecosystems: Implications for feedbacks to regional climate. *Journal of Geophysical Research: Atmospheres*, *108*(D1), 1–17. https://doi.org/10.1029/2001JD000530

Chapin, F. S., Mcguire, A. D., Randerson, J., Pielke, R., Baldocchi, D., Hobbie, S. E., … Running, S. W. (2000). Arctic and boreal ecosystems of western North America as components of the climate system. *Global Change Biology*, *6*(S1), 211–223. https://doi.org/10.1046/j.1365-2486.2000.06022.x

Chen, D., Loboda, T. V., He, T., Zhang, Y., & Liang, S. (2018). Strong cooling induced by stand-replacing fires through albedo in Siberian larch forests. *Scientific Reports*, *8*(1), 4821. https://doi.org/10.1038/s41598-018-23253-1

Chen, X., Liang, S., & Cao, Y. (2016). Satellite observed changes in the Northern Hemisphere snow cover phenology and the associated radiative forcing and feedback between 1982 and 2013. *Environmental Research Letters*, *11*(8), 084002. https://doi.org/10.1088/1748-9326/11/8/084002

Chen, X., Liang, S., Cao, Y., He, T., & Wang, D. (2015). Observed contrast changes in snow cover phenology in northern middle and high latitudes from 2001–2014. *Scientific Reports*, *5*, 16820. https://doi.org/10.1038/srep16820

Collins, W. D., Rasch, P. J., Boville, B. A., Hack, J. J., McCaa, J. R., Williamson, D. L., … Zhang, M. (2006). The formulation and atmospheric simulation of the community atmosphere model version 3 (CAM3). *Journal of Climate*, *19*(11), 2144–2161. https://doi.org/10.1175/JCLI3760.1

Daly, C., Gibson, W. P., Taylor, G. H., Johnson, G. L., & Pasteris, P. (2002). A knowledge-based approach to the statistical mapping of climate. *Climate Research*, *22*(2), 99–113. https://doi.org/10.3354/cr022099 PMID: WOS:000178833200001

Daly, C., Halbleib, M., Smith, J. I., Gibson, W. P., Doggett, M. K., Taylor, G. H., … Pasteris, P. P. (2008). Physiographically sensitive mapping of climatological temperature and precipitation across the conterminous United States. *International Journal of Climatology*, *28*(15), 2031–2064. https://doi.org/10.1002/joc.1688 PMID: WOS:000261810700004

Danielson, J. J., & Gesch, D. B. (2011). Global multi-resolution terrain elevation data 2010 (GMTED2010): U.S. geological survey open-file report, 2011–1073,26 p.

de Groot, W. J., Bothwell, P. M., Taylor, S. W., Wotton, B. M., Stocks, B. J., & Alexander, M. E. (2004). Jack pine regeneration and crown fires. *Canadian Journal of Forest Research*, *34*(8), 1634–1641. https://doi.org/10.1139/x04-073

de Groot, W. J., Cantin, A. S., Flannigan, M. D., Soja, A. J., Gowman, L. M., & Newbery, A. (2013). A comparison of Canadian and Russian boreal forest fire regimes. *Forest Ecology and Management*, *294*, 23–34. https://doi.org/10.1016/j.foreco.2012.07.033

Diner, D. (2009). "MISR level 3 component global aerosol product covering a month HDF-EOS file – Version 4". NASA Langley Atmospheric Science Data Center DAAC, 2009. https://doi.org/10.5067/terra/misr/mil3mae_l3.004

Euskirchen, E. S., Bennett, A. P., Breen, A. L., Genet, H., Lindgren, M. A., Kurkowski, T. A., … Rupp, T. S. (2016). Consequences of changes in vegetation and snow cover for climate feedbacks in Alaska and northwest Canada. *Environmental Research Letters*, *11*(10), 105003. https://doi.org/10.1088/1748-9326/11/10/105003

Flanner, M. G., Zender, C. S., Randerson, J. T., & Rasch, P. J. (2007). Present-day climate forcing and response from black carbon in snow. *Journal of Geophysical Research: Atmospheres*, *112*(D11), https://doi.org/10.1029/2006JD008003

French, N. H. F., Whitley, M. A., & Jenkins, L. K. (2016). Fire disturbance effects on land surface albedo in Alaskan tundra. *Journal of Geophysical Research: Biogeosciences*, *121*(3), 841–854. https://doi.org/10.1002/2015JG003177

Friedl, M. A., Sulla-Menashe, D., Tan, B., Schneider, A., Ramankutty, N., Sibley, A., & Huang, X. (2010). MODIS Collection 5 global land cover: Algorithm refinements and characterization of new datasets. *Remote Sensing of Environment*, *114*(1), 168–182. https://doi.org/10.1016/j.rse.2009.08.016

Genet, H., McGuire, A. D., Barrett, K., Breen, A., Euskirchen, E. S., Johnstone, J. F., … Yuan, F. (2013). Modeling the effects of fire severity and climate warming on active layer thickness and soil carbon storage of black spruce forests across the landscape in interior Alaska. *Environmental Research Letters*, *8*(4), 045016. https://doi.org/10.1088/1748-9326/8/4/045016

Gillett, N. P., Weaver, A. J., Zwiers, F. W., & Flannigan, M. D. (2004). Detecting the effect of climate change on Canadian forest fires. *Geophysical Research Letters*, *31*(18), https://doi.org/10.1029/2004GL020876

Goulden, M. L., Mcmillan, A. M. S., Winston, G. C., Rocha, A. V., Manies, K. L., Harden, J. W., & Bond-Lamberty, B. P. (2011). Patterns of NPP, GPP, respiration, and NEP during boreal forest succession. *Global Change Biology*, *17*(2), 855–871. https://doi.org/10.1111/j.1365-2486.2010.02274.x

Gruber, S. (2012). Derivation and analysis of a high-resolution estimate of global permafrost zonation. *The Cryosphere*, *6*(1), 221–233. https://doi.org/10.5194/tc-6-221-2012

H2O.ai. (Oct. 2016). *Python Interface for H2O*. Python module version 3.10.0.8. Retrieved from https://github.com/h2oai/h2o-3

Hengl, T., Mendes de Jesus, J., Heuvelink, G. B. M., Ruiperez Gonzalez, M., Kilibarda, M., Blagotić, A., … Kempen, B. (2017). SoilGrids250m: Global gridded soil information based on machine learning. *PLoS ONE*, *12*(2), e0169748. https://doi.org/10.1371/journal.pone.0169748

Hijmans, R. J., Cameron, S. E., Parra, J. L., Jones, P. G., & Jarvis, A. (2005). Very high resolution interpolated climate surfaces for global land areas. *International Journal of Climatology*, *25*(15), 1965–1978. https://doi.org/10.1002/joc.1276

Hijmans, R. J., van Etten, J., Mattiuzzi, M., Sumner, M., Greenberg, J. A., Lamigueiro, O. P., … Shortridge, A. (2014). *Package "raster"* (No. Version 2.2-31). CRAN Repository.

Hovi, A., Liang, J., Korhonen, L., Kobayashi, H., & Rautiainen, M. (2016). Quantifying the missing link between forest albedo and productivity in the boreal zone. *Biogeosciences*, *13*(21), 6015–6030. https://doi.org/10.5194/bg-13-6015-2016

Hovi, A., Lindberg, E., Lang, M. et al. (2019). Seasonal dynamics of albedo across European boreal forests – Analysis of MODIS albedo and structural metrics from airborne LiDAR. *Remote Sensing of Environment*, *224*, 365–381.

Hutchinson, M. F. (1989). A new objective method for spatial interpolation of meteorological variables from irregular networks applied to the estimation of monthly mean solar radiation, temperature, precipitation and windrun. *CSIRO Division of Water Resources Tech. Memo.*, *89*(5), 95–104.

Jafarov, E. E., Romanovsky, V. E., Genet, H., McGuire, A. D., & Marchenko, S. S. (2013). The effects of fire on the thermal stability of permafrost in lowland and upland black spruce forests of interior Alaska in a changing climate. *Environmental Research Letters*, *8*(3), 035030. https://doi.org/10.1088/1748-9326/8/3/035030

Jin, Y., Randerson, J. T., Goulden, M. L., & Goetz, S. J. (2012). Post-fire changes in net shortwave radiation along a latitudinal gradient in boreal North America. *Geophysical Research Letters*, *39*(13), https://doi.org/10.1029/2012GL051790

Johnson, E. A. (1992). *Fire and vegetation dynamics-studies from the North American boreal forest*. Cambridge, UK: Cambridge University Press.

Johnson, E. A., Miyanishi, K., & Kleb, H. (1994). The hazards of interpretation of static age structures as shown by stand reconstructions in a *Pinus contorta – Picea engelmannii* forest. *Journal of Ecology*, *82*(4), 923–931. https://doi.org/10.2307/2261455

Johnson, E. A., Miyanishi, K., & Weir, J. M. H. (1998). Wildfires in the western Canadian boreal forest: Landscape patterns and ecosystem management. *Journal of Vegetation Science*, *9*(4), 603–610. https://doi.org/10.2307/3237276

Johnstone, J. F., Chapin, F. S., Hollingsworth, T. N., Mack, M. C., Romanovsky, V., & Turetsky, M. (2010). Fire, climate change, and forest resilience in interior Alaska This article is one of a selection of papers from The Dynamics of Change in Alaska's Boreal Forests: Resilience and Vulnerability in Response to Climate Warming. *Canadian Journal of Forest Research*, *40*(7), 1302–1312. https://doi.org/10.1139/X10-061

Jorgenson, M. T., Romanovsky, V., Harden, J., Shur, Y., O'Donnell, J., Schuur, E. A. G., … Marchenko, S. (2010). Resilience and vulnerability of permafrost to climate changeThis article is one of a selection of papers from The Dynamics of Change in Alaska's Boreal Forests: Resilience and Vulnerability in Response to Climate Warming. *Canadian Journal of Forest Research*, *40*(7), 1219–1236. https://doi.org/10.1139/X10-060

Kasischke, E. S., Verbyla, D. L., Rupp, T. S., McGuire, A. D., Murphy, K. A., Jandt, R., … Turetsky, M. R. (2010). Alaska's changing fire regime — Implications for the vulnerability of its boreal forestsThis article is one of a selection of papers from The Dynamics of Change in Alaska's Boreal Forests: Resilience and Vulnerability in Response to Climate Warming. *Canadian Journal of Forest Research*, *40*(7), 1313–1324. https://doi.org/10.1139/X10-098

Kasischke, E. S., Williams, D., & Barry, D. (2002). Analysis of the patterns of large fires in the boreal forest region of Alaska. *International Journal of Wildland Fire*, *11*(2), 131–144. https://doi.org/10.1071/wf02023

Kolden, C. A., Lutz, J. A., Key, C. H., Kane, J. T., & van Wagtendonk, J. W. (2012). Mapped versus actual burned area within wildfire perimeters: Characterizing the unburned. *Forest Ecology and Management*, *286*, 38–47. https://doi.org/10.1016/j.foreco.2012.08.020

Kuhn, M., & Johnson, K. (2013). *Applied predictive modeling*. New York, NY: Springer.

Kuusinen, N., Tomppo, E., Shuai, Y., & Berninger, F. (2014). Effects of forest age on albedo in boreal forests estimated from MODIS and Landsat albedo retrievals. *Remote Sensing of Environment*, *145*, 145–153. https://doi.org/10.1016/j.rse.2014.02.005

Li, Q., Ma, M., Wu, X., & Yang, H. (2018). Snow cover and vegetation-induced decrease in global albedo from 2002 to 2016. *Journal of Geophysical Research: Atmospheres*, *123*(1), 124–138. https://doi.org/10.1002/2017JD027010

Li, Y., Wang, T., Zeng, Z., Peng, S., Lian, X., & Piao, S. (2016). Evaluating biases in simulated land surface albedo from CMIP5 global climate models. *Journal of Geophysical Research: Atmospheres*, *121*(11), 6178–6190. https://doi.org/10.1002/2016JD024774

Liu, H., & Randerson, J. T. (2008). Interannual variability of surface energy exchange depends on stand age in a boreal forest fire chronosequence. *Journal of Geophysical Research: Biogeosciences*, *113*(G1), https://doi.org/10.1029/2007JG000483

Liu, J., Schaaf, C., Strahler, A., Jiao, Z., Shuai, Y., Zhang, Q., … Dutton, E. G. (2009). Validation of Moderate Resolution Imaging Spectroradiometer (MODIS) albedo retrieval algorithm: Dependence of albedo on solar zenith angle. *Journal of Geophysical Research: Atmospheres*, *114*(D1), https://doi.org/10.1029/2008JD009969

Loranty, M. M., Berner, L. T., Goetz, S. J., Jin, Y., & Randerson, J. T. (2014). Vegetation controls on northern high latitude snow-albedo feedback: Observations and CMIP5 model simulations. *Global Change Biology*, *20*(2), 594–606. https://doi.org/10.1111/gcb.12391

Lyons, E. A., Jin, Y., & Randerson, J. T. (2008). Changes in surface albedo after fire in boreal forest ecosystems of interior Alaska assessed using MODIS satellite observations. *Journal of Geophysical Research: Biogeosciences*, *113*(G2), https://doi.org/10.1029/2007JG000606

Massey, R., Berner, L. T., Rogers, B. M., Mack, M. C., Cooperdock, S., Walker, X., & Goetz, S. J. (2019). Boreal forest deciduous fractional cover across Alaska and Canada. Publication in preparation.

Meinshausen, M., Smith, S. J., Calvin, K., Daniel, J. S., Kainuma, M. L. T., Lamarque, J.-F., … van Vuuren, D. P. (2011). The RCP greenhouse gas concentrations and their extensions from 1765 to 2300. *Climatic Change*, *109*(1), 213–241. https://doi.org/10.1007/s10584-011-0156-z

Melvin, A. M., Murray, J., Boehlert, B., Martinich, J. A., Rennels, L., & Rupp, T. S. (2017). Estimating wildfire response costs in Alaska's changing climate. *Climatic Change*, *141*(4), 783–795. https://doi.org/10.1007/s10584-017-1923-2

Mitchell, T. D., & Jones, P. D. (2005). An improved method of constructing a database of monthly climate observations and associated high-resolution grids. *International Journal of Climatology*, *25*(6), 693–712. https://doi.org/10.1002/joc.1181

Mouteva, G. O., Czimczik, C. I., Fahrni, S. M., Wiggins, E. B., Rogers, B. M., Veraverbeke, S., … Randerson, J. T. (2015). Black carbon aerosol dynamics and isotopic composition in Alaska linked with boreal fire emissions and depth of burn in organic soils. *Global Biogeochemical Cycles*, *29*(11), 1977–2000. https://doi.org/10.1002/2015GB005247

Oh, H.-R., Choi, Y.-S., Ho, C.-H., & Jeong, M.-J. (2013). Estimation of aerosol direct radiative effects for all-sky conditions from CERES and MODIS observations. *Journal of Atmospheric and Solar-Terrestrial Physics*, *102*, 311–320. https://doi.org/10.1016/j.jastp.2013.06.009

O'Halloran, T. L., Acker, S. A., Joerger, V. M., Kertis, J., & Law, B. E. (2014). Postfire influences of snag attrition on albedo and radiative forcing. *Geophysical Research Letters*, *41*(24), 9135–9142. https://doi.org/10.1002/2014GL062024

O'Halloran, T. L., Law, B. E., Goulden, M. L., Wang, Z., Barr, J. G., Schaaf, C., … Engel, V. (2012). Radiative forcing of natural forest disturbances. *Global Change Biology*, *18*(2), 555–565. https://doi.org/10.1111/j.1365-2486.2011.02577.x

Oris, F., Asselin, H., Ali, A. A., Finsinger, W., & Bergeron, Y. (2013). Effect of increased fire activity on global warming in the boreal forest. *Environmental Reviews*, *22*(3), 206–219. https://doi.org/10.1139/er-2013-0062

Payette, S. (1992). Fire as a controlling process in the North American boreal forest. In H. H. Shugart, R. Leemans, & G. B. Bonan (Eds.), *A systems analysis of the global boreal forest* (pp. 144–169). New York, NY: Cambridge University Press.

Platnick, S., Hubanks, P., Meyer, K., & King, M. D. (2015a). MODIS atmosphere L3 daily product. NASA MODIS Adaptive Processing System, Goddard Space Flight Center, USA. https://doi.org/10.5067/MODIS/MOD08_D3.006

Platnick, S., Hubanks, P., Meyer, K., & King, M. D. (2015b). MODIS atmosphere L3 monthly product. NASA MODIS Adaptive Processing System, Goddard Space Flight Center, USA. https://doi.org/10.5067/MODIS/MOD08_M3.006

Pouliot, D., & Latifovic, R. (2013). *Accuracy assessment of annual land cover time series derived from change-based updating*. Banff, Canada: Institute of Electrical and Electronics Engineers. https://doi.org/10.1109/Multi-Temp.2013.6866005

Pouliot, D., Latifovic, R., Zabcic, N., Guindon, L., & Olthof, I. (2014). Development and assessment of a 250m spatial resolution MODIS annual land cover time series (2000–2011) for the forest region of Canada derived from change-based updating. *Remote Sensing of Environment*, *140*, 731–743. https://doi.org/10.1016/j.rse.2013.10.004

R Core Team. (2012). *R: A language and environment for statistical computing*. Vienna, Austria: R Foundation for Statistical Computing.

Randerson, J. T., Liu, H., Flanner, M. G., Chambers, S. D., Jin, Y., Hess, P. G., … Zender, C. S. (2006). The impact of boreal forest fire on climate warming. *Science*, *314*(5802), 1130–1132. https://doi.org/10.1126/science.1132075

Rogers, B. M., Randerson, J. T., & Bonan, G. B. (2013). High-latitude cooling associated with landscape changes from North American boreal forest fires. *Biogeosciences*, *10*(2), 699–718. https://doi.org/10.5194/bg-10-699-2013

Rogers, B. M., Soja, A. J., Goulden, M. L., & Randerson, J. T. (2015). Influence of tree species on continental differences in boreal fires and climate feedbacks. *Nature Geoscience*, *8*(3), 228–234. https://doi.org/10.1038/ngeo2352

Rogers, B. M., Veraverbeke, S., Azzari, G., Czimczik, C. I., Holden, S. R., Mouteva, G. O., … Randerson, J. T. (2014). Quantifying fire-wide carbon emissions in interior Alaska using field measurements and Landsat imagery. *Journal of Geophysical Research: Biogeosciences*, *119*(8), 1608–1629. https://doi.org/10.1002/2014JG002657

Román, M. O., Schaaf, C. B., Lewis, P., Gao, F., Anderson, G. P., Privette, J. L., … Barnsley, M. (2010). Assessing the coupling between surface albedo derived from MODIS and the fraction of diffuse skylight over spatially-characterized landscapes. *Remote Sensing of Environment*, *114*(4), 738–760. https://doi.org/10.1016/j.rse.2009.11.014

Schaaf, C., & Wang, Z. (2015). *MCD43A1 MODIS/Terra+Aqua BRDF/Albedo model parameters daily L3 global – 500m V006*. Distributed by NASA EOSDIS Land Processes DAAC. https://doi.org/10.5067/MODIS/MCD43A1.006

Sedano, F., & Randerson, J. T. (2014). Multi-scale influence of vapor pressure deficit on fire ignition and spread in boreal forest ecosystems. *Biogeosciences*, *11*(14), 3739–3755. https://doi.org/10.5194/bg-11-3739-2014

Shell, K. M., Kiehl, J. T., Shields, C. A., Shell, K. M., Kiehl, J. T., & Shields, C. A. (2008). Using the radiative kernel technique to calculate climate feedbacks in NCAR's community atmospheric model. *Journal of Climate*, *21*(10), 2269–2282. https://doi.org/10.1175/2007JCLI2044.1

Shenoy, A., Johnstone, J. F., Kasischke, E. S., & Kielland, K. (2011). Persistent effects of fire severity on early successional forests in interior Alaska. *Forest Ecology and Management*, *261*(3), 381–390. https://doi.org/10.1016/j.foreco.2010.10.021

Shugart, H. H., Leemans, R., & Bonan, G. B. (1992). *A systems analysis of the global boreal forest*. Cambridge University Press.

Solvik, K., Potter, S., Erb, A. M., Roman, M., Schaaf, C., Sun, Q., …Rogers, B. M. (2019). ABoVE: MODIS-derived daily mean blue sky albedo for northern North America, 2000–2017. ORNL DAAC, Oak Ridge, Tennessee, USA, https://doi.org/10.3334/ORNLDAAC/1605

Stocks, B. J., & Martell, D. L. (2016). Forest fire management expenditures in Canada: 1970–2013. *The Forestry Chronicle*, *92*(03), 298–306. https://doi.org/10.5558/tfc2016-056

Stocks, B. J., Mason, J. A., Todd, J. B., Bosch, E. M., Wotton, B. M., Amiro, B. D., … Skinner, W. R. (2002). Large forest fires in Canada, 1959–1997. *Journal of Geophysical Research: Atmospheres*, *108*(D1), 5–12. https://doi.org/10.1029/2001JD000484

Taylor, K. E., Stouffer, R. J., Meehl, G. A., Taylor, K. E., Stouffer, R. J., & Meehl, G. A.. (2012). An overview of CMIP5 and the experiment design. *Bulletin of the American Meteorological Society*, *93*(4), 485–498. https://doi.org/10.1175/BAMS-D-11-00094.1

Trugman, A. T., Fenton, N. J., Bergeron, Y., Xu, X., Welp, L. R., & Medvigy, D. (2016). Climate, soil organic layer, and nitrogen jointly drive forest development after fire in the North American boreal zone: CLIMATE AND SOIL DRIVE BOREAL CARBON. *Journal of Advances in Modeling Earth Systems*, *8*(3), 1180–1209. https://doi.org/10.1002/2015MS000576

Turetsky, M. R., Kane, E. S., Harden, J. W., Ottmar, R. D., Manies, K. L., Hoy, E., & Kasischke, E. S. (2011). Recent acceleration of biomass burning and carbon losses in Alaskan forests and peatlands. *Nature Geoscience*, *4*(1), 27–31. https://doi.org/10.1038/ngeo1027

Veraverbeke, S., Rogers, B. M., Goulden, M. L., Jandt, R. R., Miller, C. E., Wiggins, E. B., & Randerson, J. T. (2017). Lightning as a major driver of recent large fire years in North American boreal forests. *Nature Climate Change*, *7*(7), 529–534. https://doi.org/10.1038/nclimate3329

Veraverbeke, S., Rogers, B. M., & Randerson, J. T. (2015). Daily burned area and carbon emissions from boreal fires in Alaska. *Biogeosciences*, *12*(11), 3579–3601. https://doi.org/10.5194/bg-12-3579-2015

Viereck, L. A. (1973). Wildfire in the taiga of Alaska. *Quaternary Research*, *3*(3), 465–495. https://doi.org/10.1016/0033-5894(73)90009-4

Walker, X. J., Rogers, B. M., Baltzer, J. L., Cumming, S. G., Day, N. J., Goetz, S. J., … Mack, M. C. (2018). Cross-scale controls on carbon emissions from boreal forest megafires. *Global Change Biology*, *24*(9), 4251–4265. https://doi.org/10.1111/gcb.14287

Wang, T., Hamann, A., Spittlehouse, D., & Carroll, C. (2016). Locally downscaled and spatially customizable climate data for historical and future periods for North America. *PLoS ONE*, *11*(6), e0156720. https://doi.org/10.1371/journal.pone.0156720

Wang, Z., Erb, A. M., Schaaf, C. B., Sun, Q., Liu, Y., Yang, Y., … Román, M. O. (2016). Early spring post-fire snow albedo dynamics in high latitude boreal forests using Landsat-8 OLI data. *Remote Sensing of Environment*, *185*, 71–83. https://doi.org/10.1016/j.rse.2016.02.059

Wang, K., Liang, S., Schaaf, C. L., & Strahler, A. H. (2010). Evaluation of moderate resolution imaging spectroradiometer land surface visible and shortwave albedo products at FLUXNET sites. *Journal of Geophysical Research: Atmospheres*, *115*(D17). https://doi.org/10.1029/2009JD013101

Wang, Z., Schaaf, C. B., Chopping, M. J., Strahler, A. H., Wang, J., Román, M. O., … Shuai, Y. (2012). Evaluation of Moderate-resolution Imaging Spectroradiometer (MODIS) snow albedo product (MCD43A) over tundra. *Remote Sensing of Environment*, *117*, 264–280. https://doi.org/10.1016/j.rse.2011.10.002

Wang, Z., Schaaf, C. B., Strahler, A. H., Chopping, M. J., Román, M. O., Shuai, Y., … Fitzjarrald, D. R. (2014). Evaluation of MODIS albedo product (MCD43A) over grassland, agriculture and forest surface types during dormant and snow-covered periods. *Remote Sensing of Environment*, *140*, 60–77. https://doi.org/10.1016/j.rse.2013.08.025

Wang, Z., Schaaf, C. B., Sun, Q., Shuai, Y., & Román, M. O. (2018). Capturing rapid land surface dynamics with Collection V006 MODIS BRDF/NBAR/Albedo (MCD43) products. *Remote Sensing of Environment*, *207*, 50–64. https://doi.org/10.1016/j.rse.2018.02.001

Ward, D. S., Kloster, S., Mahowald, N. M., Rogers, B. M., Randerson, J. T., & Hess, P. G. (2012). The changing radiative forcing of fires: Global model estimates for past, present and future. *Atmospheric Chemistry and Physics*, *12*(22), 10857–10886. https://doi.org/10.5194/acp-12-10857-2012

Whitman, E., Parisien, M.-A., Thompson, D. K., & Flannigan, M. D. (2018). Topoedaphic and forest controls on post-fire vegetation assemblies are modified by fire history and burn severity in the Northwestern Canadian boreal forest. *Forests*, *9*(3), 151. https://doi.org/10.3390/f9030151

Wolfe, J. A. (1979). *Temperature parameters of humid to mesic forests of Eastern Asia and relation to forests of other regions of the Northern Hemisphere and Australasia: analysis of temperature data from more than 400 stations in Eastern Asia* (U.S. Geological Survey Professional Paper No. 1106). Washington, DC: US Dep. Int.

Wooster, M. J., & Zhang, Y. H. (2004). Boreal forest fires burn less intensely in Russia than in North America. *Geophysical Research Letters*, *31*(20), https://doi.org/10.1029/2004GL020805

Yoshikawa, K., Bolton, W. R., Romanovsky, V. E., Fukuda, M., & Hinzman, L. D. (2002). Impacts of wildfire on the permafrost in the boreal forests of Interior Alaska. *Journal of Geophysical Research: Atmospheres*, *108*(D1), 4–14. https://doi.org/10.1029/2001JD000438

Young, A. M., Higuera, P. E., Duffy, P. A., & Hu, F. S. (2017). Climatic thresholds shape northern high-latitude fire regimes and imply vulnerability to future climate change. *Ecography*, *40*(5), 606–617. https://doi.org/10.1111/ecog.02205

Yu, H., Kaufman, Y. J., Chin, M., Feingold, G., Remer, L. A., Anderson, T. L., … Zhou, M. (2006). A review of measurement-based assessments of the aerosol direct radiative effect and forcing. *Atmospheric Chemistry and Physics*, *6*, 613–666. https://doi.org/10.5194/acp-6-613-2006

SUPPORTING INFORMATION

Additional supporting information may be found online in the Supporting Information section.

How to cite this article: Potter S, Solvik K, Erb A, et al. Climate change decreases the cooling effect from postfire albedo in boreal North America. *Glob Change Biol*. 2019;00:1–16. https://doi.org/10.1111/gcb.14888